Parametric resonance magnetometer based on elliptically polarized light yielding three-axis measurement with isotropic sensitivity

Gwenael Le Gal, Laure-Line Rouve, Agustin Palacios-Laloy

Parametric resonance magnetometer based on elliptically polarized light yielding three-axis measurement with isotropic sensitivity

Cite as: XXXXXXXXXX
Submitted: XXXXXXX
Published online: XXXXXXXX

Gwenael Le Gal,[1,2] Laure-Line Rouve,[2] Agustin Palacios-Laloy[1,*]

[1]Univ. Grenoble Alpes, CEA, Leti, F-38000 Grenoble, France
[2]Univ. Grenoble Alpes, CNRS, Grenoble INP, G2Elab, 21 rue des martyrs, Grenoble 38000, France
*Corresponding author: Agustin.palacioslaloy@cea.fr

Abstract

We present here a parametric resonance magnetometer scheme based on elliptically polarized pumping light and two radio-frequency fields applied along the two optical pumping directions. At optimum ellipticity and radio-frequency fields amplitudes the three components of the magnetic field are measured with an isotropic sensitivity. Compared to the usual alignment-based parametric resonance magnetometers, the sensitivity is degraded by a factor 2 for two components of the magnetic field but improved by a factor 9 for the third one. The open-loop bandwidth was measured to be greater than 1 kHz for the three axes. This magnetometer configuration could be particularly interesting for geophysics and biomedical imaging.

Currently, optically pumped magnetometers (OPMs) can reach excellent sensitivities similar to SQUIDs [1,2] but without requiring cryogenics. This opens new prospects to precisely measure magnetic fields in studies of fundamental symmetries [3], space exploration [4] and geophysics [5]. For instance, a vector measurement of the magnetic field with sensitivity < 1 pT/√Hz and high bandwidth (> 1 kHz) is desirable for the detection of local phenomena in the Earth's ionosphere [6–8]. OPMs also open new perspectives for magnetic imaging of biological currents in magnetocardiography (MCG) [9,10], and magnetoencephalography (MEG) [11–13]. Both for MEG and MCG, some recent studies suggest that a tri-axial magnetometer would improve the accuracy of source reconstruction [14,15], as well as the noise rejection [16], as far as the sensitivity is isotropic [15].

Such an isotropic sensitivity is not straightforward for OPMs, due to the symmetry breaking by the polarization of the pumping light. For instance magnetometers based on the Hanle effect allow a real-time vector measurement of the components of the magnetic field [1,17] which are orthogonal to the characteristic direction of pumping. In order to use a single light beam, parametric resonances magnetometers (PRM) are often used instead [18]. Fig. 1(a) shows a typical PRM based on alkali atoms [19–21], optically pumped toward an oriented state, i.e. a state with $\langle S_k \rangle \neq 0$ where $\vec{k}$ is the propagation direction of the circularly polarized pump beam. Two orthogonal radio frequency (RF) fields allow to measure the two components of the magnetic field parallel to them [19,22–24]. Unlike the Hanle effect magnetometer, the third component, parallel to $\vec{k}$, can be measured thanks to non-secular terms [22] but with a sensitivity much worse than the others.

An atomic state with F > 1/2 can be pumped using circularly polarized light toward an oriented state, or, using linearly polarized light, toward an aligned state (i.e. a state with $\langle 3S_e^2 - \vec{S}^2 \rangle \neq 0$ where $\vec{e}$ is the direction of the pump-light electric field $\vec{E}_0$ [25]). Using alignment instead of orientation in a PRM (Fig. 1(b)) yields a better sensitivity for the worst resolved axis [23], which in this case is parallel to $\vec{e}$, relatively to the two other axes.Such PRMs based on the 2^3S_1 ^{4}He metastable state (F = S = 1) proved their ability to detect biomagnetic signals both in MCG [10] and MEG [12].

As it is usual in magnetometry, we refer to sensitivity as the intrinsic noise of the sensor. When this sensitivity is limited by optical noise which is almost white at the frequencies of interest, as it is now for ^{4}He alignment-based PRMs [26], it varies as [27]:

$$\delta B_{sn} = \frac{\delta I}{|dI_d/dB_i|} \quad (1)$$

Where $|dI_d/dB_i|$ is the slope of the dispersive parametric resonance signal and δI the optical noise. B_i refers to either B_x, B_y or B_z. Within this assumption, maximizing the dispersive signal slope is equivalent to optimizing the magnetometer sensitivity.

We introduce here a ^{4}He PRM configuration based on elliptically polarized pumping light that delivers vector measurement of the three components of the magnetic field with isotropic slopes. Indeed using elliptically polarized pumping light one can simultaneously prepare both an orientation and an alignment in the atomic ensemble, with a ratio fixed by the light ellipticity. Since $\vec{e}$ and $\vec{k}$ are orthogonal, and since the evolutions of orientation and alignment within a magnetic field are decoupled [23], we studied if their combination yields well resolved measurements of the three components of the magnetic field.

A first important parameter to set for obtaining isotropic slopes is the pump light ellipticity. Since the zero-field parametric resonances can be interpreted as the Hanle resonances of the atom dressed by the RF fields we can study the effect of light ellipticity on Hanle effect resonances. Indeed, the dressing only leads to a ponderation of the slopes by factors comprising Bessel functions [22,23]. The slope of a PRM is proportional to $A = a/\Gamma^2$ [22], where Γ is the half-width-half-maximum (HWHM) of the Hanle resonance and a/Γ is its amplitude. We investigated experimentally the variation of A as a function of the light ellipticity. The experimental setup for doing so is shown in Fig. 1(d). It comprises a 1-cm diameter and 1-cm length cylindrical cell filled with 9-torr high purity helium-4, where the metastable state is populated using a high-frequency (HF) capacitively coupled discharge. An external cavity laser diode (Sacher Cheetah TEC 50) generates the pump beam. To keep it tuned with ^{4}He D_0 transition (at 1083.205 nm) a wavelength-meter (HighFiness WS-7) locks the laser diode temperature. The laser is collimated to 7-mm waist, and goes through a linear polarizer with transmission axis set at an angle φ from the $\vec{y}$ axis, and a $\lambda/4$ zero-order waveplate (Thorlabs WPQ10M-1064), with its fast axis parallel to the $\vec{y}$ axis. The optical power is set to ~250 µW at cell input. The helium cell is placed inside two sets of triaxial coils: the inner one generating the RF fields, the outer one generating the magnetic field sweeps. The cell and coils are put inside a five-layer µ-metal magnetic shield. After crossing the cell, a lens focuses the light on an In-Ga-As photodiode, connected to a homemade transimpedance amplifier with 23.8 kΩ gain. We measure the DC photodetection signal while sweeping sequentially each component of the magnetic field of ±300 nT, with the others set to zero. Here no RF fields are applied. The Fig. 1(e) shows the experimental dependency.

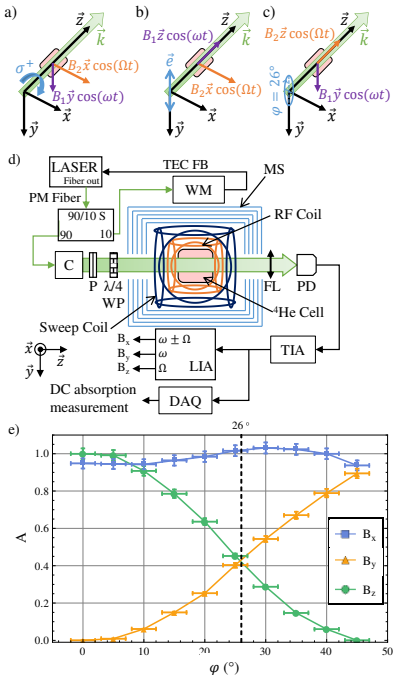

FIG. 1. (a,b,c) Schematic representation of the usual orientation-, alignment-, and elliptically-polarized-light-based PRMs configurations, respectively. (d) Experimental setup. TEC FB: TEC feedback, 90/10 S: 90/10 Splitter, WM: Wavelength-meter, MS: Magnetic shield, C: Collimator, P: Polarizer, WP: Waveplate, FL: Focusing lens, PD: Photodiode, TIA: Transimpedance amplifier, LIA: Lock-in amplifier, DAQ: DAQmx board. The LIA outputs refer to the configuration of Fig. 1 (c). (e) Experimental dependency of the amplitude (a/Γ) over HWHM (Γ) ratio of Hanle resonances for each component of the magnetic field as a function of the pumping light ellipticity, which can be shown to be equal to φ.

When the ellipticity is different from 0° (linear polarization) or 45° (circular polarization) one can observe Hanle resonances with respect to all components of the magnetic field.

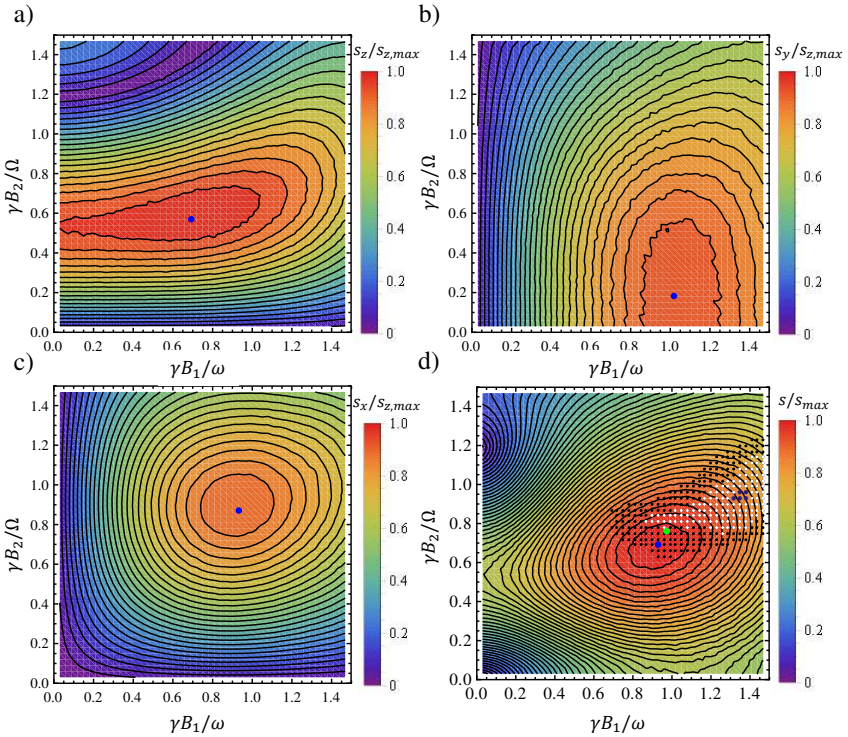

FIG. 2. (a, b, c) Experimentally measured variation of the slopes (normalized with the highest value reached among the three axes $s_{z,max}$) to the B_z, B_y and B_x components, respectively as a function of the RF amplitudes. These range from 16 nT_p to 802.5 nT_p ($\Leftrightarrow \gamma B_2/\Omega = 0.03$ to 1.5 where $\gamma = 2\pi \times 28$ Hz/nT is the ^4He 2^3S_1 state gyromagnetic ratio) for the slow RF field and from 42.8 nT_p to 2140 nT_p ($\Leftrightarrow \gamma B_1/\omega = 0.03$ to 1.5) for the fast RF field. The blue dots show the setting yielding maximum slope to each component $s_{z,max}$, $s_{y,max}$ and $s_{x,max}$, respectively. (d) Normalized quadratic sum of the three slopes. The blue dot shows the setting yielding the maximum s. The black dotted area corresponds to the region where the slope for each axis complies to $0.3 < I_x$ & I_y & $I_z < 0.37$. The white dotted area complies to $0.31 < I_x$ & I_y & $I_z < 0.35$ and the purple dotted area to $0.325 < I_x$ & I_y & $I_z < 0.335$. The green dot shows the experimentally determined setting where $I_x \approx I_y \approx I_z \approx 0.33$ while having maximal slope for each axis.

At $\varphi = 26°$, A is equal for the Hanle resonances observed by sweeping B_y and B_z, and higher for the Hanle resonance observed by sweeping B_x. This ellipticity seems therefore to be a good starting point for reaching isotropic slopes, as it is the best compromise to have the best slope to the three components of the magnetic field.

We now move to PRM scheme, by adding RF fields. We consider the setup of Fig. 1(c): an elliptically polarized pump light with $\varphi = 26°$ ellipticity propagates along $\vec{z}$, with the major axis of the polarization ellipse parallel to $\vec{y}$. Two RF fields $B_1\vec{y}\cos(\omega t)$ and $B_2\vec{z}\cos(\Omega t)$ are applied, with $\omega \gg \Omega$ [22,23], $\omega/2\pi = 40$ kHz and $\Omega/2\pi = 15$ kHz. Note that here, as shown in Fig. 1(a,b,c), unlike the usual orientation- or alignment-based PRMs [19,22,23], the RF fields are applied along the optical pumping characteristic directions: the propagation direction $\vec{k} \parallel \vec{z}$ (for the orientation) and the major axis of the polarization ellipse $\vec{y}$ (for the alignment). This choice is made because applying a RF field transverse to a given component of the magnetic field degrades the slope to this component. From Fig. 1(e), we see that the slope to B_x is larger than the ones to B_y and B_z at $\varphi = 26°$. It is therefore better to degrade less those latter slopes and more the former for obtaining isotropy. More detailed reasons for this choice as well as the theoretical model accounting for the dynamics of atoms optically pumped using

elliptically polarized light and subject to several RF fields will be discussed elsewhere.

In order to find the optimal RF amplitudes we first measure the slope of the PRM to each component of $\vec{B}$, as a function of the amplitudes of the two RF fields. We perform sweeps of ± 90 nT for each component of the field with the other set to zero. In addition to the experimental setup previously described, the photodetection signal is demodulated with a Zürich MFLI lock-in amplifier, at 40 kHz to measure the B_y component, at 15 kHz for the B_z component and at 25 kHz ($\omega \pm \Omega$ [23]) for the B_x component. The slopes $s_{x,y,z}$, obtained by a linear fit around the null field, are shown in Fig. 2(a,b,c).

Among all the slopes, the largest is the one to the B_z component at $\gamma B_1/\omega = 0.69$ and $\gamma B_2/\Omega = 0.57$. The slope to B_y reaches its maximum for $\gamma B_1/\omega = 1.02$ and $\gamma B_1/\Omega = 0.18$. Finally, the slope to B_x is maximum for $\gamma B_1/\omega = 0.93$ and $\gamma B_2/\Omega = 0.87$. The maximum slopes to B_y and B_x are 93 % and 90 % of the maximum to B_z.

According to equation (1), a figure of merit of the overall intrinsic noise is $s = \left(s_x^2 + s_y^2 + s_z^2\right)^{1/2}$. Its dependence is shown in Fig. 2(d). s is maximum for $\gamma B_1/\omega = 0.93$ and $\gamma B_2/\Omega = 0.69$ (blue dot in Fig. 2(d)). However, at this maximum the three slopes, s_x, s_y and s_z, are not equal. Experimentally, we determine that the optimal isotropic sensitivity is obtained for $\gamma B_1/\omega = 0.97$ and $\gamma B_2/\Omega = 0.76$ (green dot in Fig. 2(d)), which is in the vicinity of the isotropic condition $I_x \approx I_y \approx I_z \approx 0.33$ where $I_{x,y,z} = |s_{x,y,z}|/(|s_x| + |s_y| + |s_z|)$.

To compare the proposed scheme with the alignment-based PRM, we record the parametric resonance signals for the two configurations sequentially on the same experimental setup (Fig. 3). For alignment-based PRM, the pumping light is linearly polarized along $\vec{y}$ ($\varphi = 0°$). The 40 kHz RF field is applied along $\vec{z}$ and the 15 kHz one along $\vec{x}$, with amplitudes so that $\gamma B_1/\omega = 0.41$ and $\gamma B_2/\Omega = 0.46$, respectively, yielding $s_x = s_z$ [23]. In the proposed scheme $\varphi = 26°$ and the RF amplitudes are set at optimum isotropic setting ($\gamma B_1/\omega = 0.97$ and $\gamma B_2/\Omega = 0.76$). One can see that for the two well-resolved axes of the alignment-based PRM (B_x and B_z), the slopes are degraded by a factor 2.5 and 2.2, respectively, in the proposed scheme. The slope of the third axis, B_y, is however 9 times greater. Additionally, the open-loop bandwidth is measured of be close to 1.5 kHz, as shown in Fig. 3(d) for both the elliptically-polarized-light-based PRM and the alignment based PRM. In the alignment-based PRM configuration the sensitivity on our experimental setup are close to 210 fT/√Hz for B_x and B_z, and 4650 fT/√Hz for B_y. In the elliptically-polarized-light-based configuration, we measure 500 fT/√Hz for the three

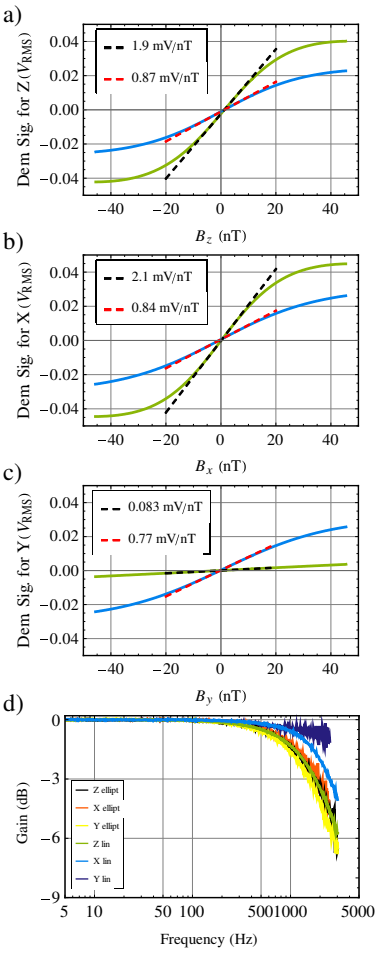

FIG. 3. (a,b,c) Parametric resonance signals for the three components of the magnetic field and the low field linear fits, for the alignment-based standard PRM configuration (green and black dashed lines) and for the elliptically-polarized-light-based PRM configuration (blue and red dashed lines). Green curves are taken for $\gamma B_1/\omega = 0.41$ and $\gamma B_2/\Omega = 0.46$ and blue curves are acquired for $\gamma B_1/\omega = 0.97$ and $\gamma B_2/\Omega = 0.76$. The natural magnetic field offset along each component is compensated for all curves by applying $B_{z,0} = 0$ nT, $B_{x,0} = 13.3$ nT and $B_{y,0} = 9.4$ nT.(d) Measured bandwidth for the three axes in both magnetometer schemes, recorded by sweeping in frequency a 2 nT_{RMS} field. The laser frequency locking is disabled for bandwidth measurement.

components. These values could be strongly improved (a factor 5) with a setup optimized for noise measurements, as the one used in [26]. Nevertheless, those sensitivities closely follow the relative slopes of the axes shown in Fig. 3(a,b,c).

In the proposed scheme, the wavelength of light has to be precisely tuned to the ^{4}He D_0 transition. Otherwise, since the light is partially circularly polarized, it causes a vector light-shift along the propagation direction $\vec{z}$ [28], resulting in an offset and possibly increased noise on B_z. Another undesirable effect of such a detuning is the so-called orientation-to-alignment conversion (AOC) [29,30] which comes from the linearly polarized fraction of the pumping light. In the usual alignment-based PRM, the AOC effect does not affect the accuracy of the sensor, only possibly causing a broadening of the resonances and loss of sensitivity [30]. In the proposed scheme, we have observed that the AOC effect breaks the isotropy of the sensitivity and the odd-symmetry of the parametric resonance signals around the null field.

In conclusion, we introduced here a PRM scheme based on elliptically polarized pumping light. With two RF fields set along the propagation and polarization directions of the pump light, it is possible to obtain a three-axis measurement of the magnetic field with isotropic sensitivity for photon shot noise limited magnetometer. The slopes of this scheme are degraded by a factor 2.5 (2.2) for the B_x (B_z) component compared to the usual alignment-based PRMs. The slope to the B_y component is improved by a factor 9. The measured sensitivities are consistent with those changes in the slopes between the two configurations. With the recent improvement in the ^{4}He PRMs sensitivity below 50 fT/√Hz [26], we expect vector triaxial measurements with an isotropic sensitivity of 100 fT/√Hz, while keeping a bandwidth close to 1.5 kHz.

In addition to its direct applications, isotropic sensitivity also opens interesting perspectives for building arrays of magnetometers operating in closed-loop configuration [31,32]. Indeed, it avoids injecting the high magnetic noise of the worst resolved axis on the other axes of the neighbor magnetometers.

Acknowledgments

We acknowledge technical help of W. Fourcault, cell filling by F. Alcouffe, and interesting discussions with E. Labyt, J.M. Léger, M. Le Prado, T. Jager and F. Bertrand. G.L.G acknowledges the CEA-LETI DSYS Ph.D. funding.

Data Availability

The data that support the findings of this study are available from the corresponding authors upon reasonable request.

References

[1] J. C. Allred, R. N. Lyman, T. W. Kornack, and M. V. Romalis, *High-Sensitivity Atomic Magnetometer Unaffected by Spin-Exchange Relaxation*, Phys. Rev. Lett. **89**, 130801 (2002).

[2] A. Grosz, M. J. Haji-Sheikh, and S. C. Mukhopadhyay, editors , *High Sensitivity Magnetometers* (Springer Berlin Heidelberg, New York, NY, 2016).

[3] C. Abel, S. Afach, N. J. Ayres, C. A. Baker, G. Ban, G. Bison, K. Bodek, V. Bondar, M. Burghoff, E. Chanel, Z. Chowdhuri, P.-J. Chiu, B. Clement, C. B. Crawford, M. Daum, S. Emmenegger, L. Ferraris-Bouchez, M. Fertl, P. Flaux, B. Franke, A. Fratangelo, P. Geltenbort, K. Green, W. C. Griffith, M. van der Grinten, Z. D. Grujić, P. G. Harris, L. Hayen, W. Heil, R. Henneck, V. Hélaine, N. Hild, Z. Hodge, M. Horras, P. Iaydjiev, S. N. Ivanov, M. Kasprzak, Y. Kermaidic, K. Kirch, A. Knecht, P. Knowles, H.-C. Koch, P. A. Koss, S. Komposch, A. Kozela, A. Kraft, J. Krempel, M. Kuźniak, B. Lauss, T. Lefort, Y. Lemière, A. Leredde, P. Mohanmurthy, A. Mtchedlishvili, M. Musgrave, O. Naviliat-Cuncic, D. Pais, F. M. Piegsa, E. Pierre, G. Pignol, C. Plonka-Spehr, P. N. Prashanth, G. Quéméner, M. Rawlik, D. Rebreyend, I. Rienäcker, D. Ries, S. Roccia, G. Rogel, D. Rozpedzik, A. Schnabel, P. Schmidt-Wellenburg, N. Severijns, D. Shiers, R. Tavakoli Dinani, J. A. Thorne, R. Virot, J. Voigt, A. Weis, E. Wursten, G. Wyszynski, J. Zejma, J. Zenner, and G. Zsigmond, *Measurement of the Permanent Electric Dipole Moment of the Neutron*, Phys. Rev. Lett. **124**, 081803 (2020).

[4] J.-M. Léger, T. Jager, F. Bertrand, G. Hulot, L. Brocco, P. Vigneron, X. Lalanne, A. Chulliat, and I. Fratter, *In-Flight Performance of the Absolute Scalar Magnetometer Vector Mode on Board the Swarm Satellites*, Earth Planets Space **67**, 57 (2015).

[5] P. Vigneron, G. Hulot, N. Olsen, J.-M. Léger, T. Jager, L. Brocco, O. Sirol, P. Coïsson, X. Lalanne, A. Chulliat, F. Bertrand, A. Boness, and I. Fratter, *A 2015 International Geomagnetic Reference Field (IGRF) Candidate Model Based on Swarm's Experimental Absolute Magnetometer Vector Mode Data*, Earth Planets Space **67**, 95 (2015).

[6] U. Ali Ahmad, Y. Kasahara, S. Matsuda, M. Ozaki, and Y. Goto, *Automatic Detection of Lightning Whistlers Observed by the Plasma Wave Experiment Onboard the Arase Satellite Using the OpenCV Library*, Remote Sens. **11**, 1785 (2019).

[7] C. D. Beggan and M. Musur, *Observation of Ionospheric Alfvén Resonances at 1-30 Hz and Their Superposition With the Schumann*

Resonances, J. Geophys. Res. Space Phys. **123**, 4202 (2018).

[8] Y. Yokoyama, S. Taguchi, T. Iyemori, and K. Hosokawa, *The Quasipersistent Feature of Highly Structured Field-Aligned Currents in the Duskside Auroral Oval: Conjugate Observation Via Swarm Satellites and a Ground All-Sky Imager*, J. Geophys. Res. Space Phys. **125**, (2020).

[9] A. Weis, G. Bison, N. Castagna, S. Cook, A. Hofer, M. Kasprzak, P. Knowles, and J.-L. Schenker, *Mapping the Cardiomagnetic Field with 19 Room Temperature Second-Order Gradiometers*, IFMBE Proc. **28**, 58 (2010).

[10] S. Morales, M. C. Corsi, W. Fourcault, F. Bertrand, G. Cauffet, C. Gobbo, F. Alcouffe, F. Lenouvel, M. Le Prado, F. Berger, G. Vanzetto, and E. Labyt, *Magnetocardiography Measurements with 4 He Vector Optically Pumped Magnetometers at Room Temperature*, Phys. Med. Biol. **62**, 7267 (2017).

[11] H. Xia, A. Ben-Amar Baranga, D. Hoffman, and M. V. Romalis, *Magnetoencephalography with an Atomic Magnetometer*, Appl. Phys. Lett. **89**, 211104 (2006).

[12] E. Labyt, M. C. Corsi, W. Fourcault, A. Palacios-Laloy, F. Bertrand, F. Lenouvel, G. Cauffet, M. Le Prado, F. Berger, and S. Morales, *Magnetoencephalography With Optically Pumped 4He Magnetometers at Ambient Temperature*, IEEE Trans. Med. Imaging **38**, 90 (2019).

[13] M. Petrenko, S. Dmitriev, A. Pazgalev, A. Ossadtchi, and A. Vershovskii, Towards the Non-Zero Field Cesium Magnetic Sensor Array for Magnetoencephalography, preprint, 2021.

[14] J. Haueisen, K. Fleissig, D. Strohmeier, T. Elsarnagawy, R. Huonker, M. Liehr, and O. W. Witte, *Reconstruction of Quasi-Radial Dipolar Activity Using Three-Component Magnetic Field Measurements*, Clin. Neurophysiol. **123**, 1581 (2012).

[15] J. Iivanainen, M. Stenroos, and L. Parkkonen, *Measuring MEG Closer to the Brain: Performance of on-Scalp Sensor Arrays*, NeuroImage **147**, 542 (2017).

[16] J. Nurminen, S. Taulu, J. Nenonen, L. Helle, J. Simola, and A. Ahonen, *Improving MEG Performance With Additional Tangential Sensors*, IEEE Trans. Biomed. Eng. **60**, 2559 (2013).

[17] G. Le Gal, G. Lieb, F. Beato, T. Jager, H. Gilles, and A. Palacios-Laloy, *Dual-Axis Hanle Magnetometer Based on Atomic Alignment with a Single Optical Access*, Phys. Rev. Appl. **12**, 064010 (2019).

[18] C. Cohen-Tannoudji, J. Dupont-Roc, S. Haroche, and F. Laloë, *Diverses Résonances de Croisement de Niveaux Sur Des Atomes Pompés Optiquement En Champ Nul. I. Théorie*, Rev. Phys. Appliquée **5**, 95 (1970).

[19] V. Shah, J. Osborne, J. Orton, and O. Alem, *Fully Integrated, Standalone Zero Field Optically Pumped Magnetometer for Biomagnetism*, in *Steep Dispersion Engineering and Opto-Atomic Precision Metrology XI*, edited by S. M. Shahriar and J. Scheuer (SPIE, San Francisco, United States, 2018), p. 51.

[20] C. Cohen-Tannoudji, J. Dupont-Roc, S. Haroche, and F. Laloë, *Diverses Résonances de Croisement de Niveaux Sur Des Atomes Pompés Optiquement En Champ Nul. II. Applications à La Mesure de Champs Faibles*, Rev. Phys. Appliquée **5**, 102 (1970).

[21] D. Sheng, A. R. Perry, S. P. Krzyzewski, S. Geller, J. Kitching, and S. Knappe, *A Microfabricated Optically-Pumped Magnetic Gradiometer*, Appl. Phys. Lett. **110**, 031106 (2017).

[22] J. Dupont-Roc, *Étude Théorique de Diverses Résonances Observables En Champ Nul Sur Des Atomes " Habillés " Par Des Photons de Radiofréquence*, J. Phys. **32**, 135 (1971).

[23] F. Beato, E. Belorizky, E. Labyt, M. Le Prado, and A. Palacios-Laloy, *Theory of a He 4 Parametric-Resonance Magnetometer Based on Atomic Alignment*, Phys. Rev. A **98**, (2018).

[24] R. Slocum and B. Marton, *Measurement of Weak Magnetic Fields Using Zero-Field Parametric Resonance in Optically Pumped He⁴*, IEEE Trans. Magn. **9**, 221 (1973).

[25] Y. Shi and A. Weis, *Cesium Alignment Produced by Pumping with Unpolarized Light*, Eur. Phys. J. D **72**, (2018).

[26] W. Fourcault, R. Romain, G. Le Gal, F. Bertrand, V. Josselin, M. Le Prado, E. Labyt, and A. Palacios-Laloy, *Helium-4 Magnetometers for Room-Temperature Biomedical Imaging: Toward Collective Operation and Photon-Noise Limited Sensitivity*, Opt. Express (2021).

[27] V. Schultze, B. Schillig, R. IJsselsteijn, T. Scholtes, S. Woetzel, and R. Stolz, *An Optically Pumped Magnetometer Working in the Light-Shift Dispersed Mz Mode*, Sensors **17**, 561 (2017).

[28] C. Cohen-Tannoudji and J. Dupont-Roc, *Experimental Study of Zeeman Light Shifts in Weak Magnetic Fields*, Phys. Rev. A **5**, 968 (1972).

[29] W. Happer and B. S. Mathur, *Effective Operator Formalism in Optical Pumping*, Phys. Rev. **163**, 12 (1967).

[30] F. Beato and A. Palacios-Laloy, *Second-Order Effects in Parametric-Resonance Magnetometers Based on Atomic Alignment*, EPJ Quantum Technol. **7**, 9 (2020).

[31] I. A. Sulai, Z. J. DeLand, M. D. Bulatowicz, C. P. Wahl, R. T. Wakai, and T. G. Walker, *Characterizing Atomic Magnetic Gradiometers for Fetal Magnetocardiography*, Rev. Sci. Instrum. **90**, 085003 (2019).

[32] R. Wyllie, M. Kauer, R. T. Wakai, and T. G. Walker, *Optical Magnetometer Array for Fetal Magnetocardiography*, Opt. Lett. **37**, 2247 (2012).